

ANALYSIS OF SPATIAL STRUCTURE OF THE SPICA H II REGION

J.-W. PARK^{1,2}, K.-W. MIN¹, K.-I. SEON³, W. HAN³, AND J. EDELSTEIN⁴

Draft version November 15, 2018

ABSTRACT

Far ultraviolet (FUV) spectral images of the Spica H II region are first presented here for the Si II* $\lambda 1533.4$ and Al II $\lambda 1670.8$ lines and then compared with the optical H α image. The H α and Si II* images show enhanced emissions in the southern part of the H II region where H I density increases outwards. This high density region, which we identify as part of the “interaction ring” of the Loop I superbubble and the Local Bubble, seems to bound the southern H II region. On the other hand, the observed profile of Al II shows a broad central peak, without much difference between the northern and southern parts, which we suspect results from multiple resonant scattering. The extended tails seen in the radial profiles of the FUV intensities suggest that the nebula may be embedded in a warm ionized gas. Simulation with a spectral synthesis code yields the values of the Lyman continuum luminosity and the effective temperature of the central star similar to previous estimates with $10^{46.2}$ photons s^{-1} and 26,000 K, respectively, but the density of the northern H II region, 0.22 cm^{-3} , is much smaller than previous estimates for the H α brightest region.

Subject headings: ISM: individual (Spica) — H II region — ultraviolet: ISM

1. INTRODUCTION

H II regions are generally located in the vicinity of OB stars because these hot stars can produce strong ultraviolet radiation, thereby photoionizing hydrogen atoms in the region. The energy balance between photoelectrons and forbidden line cooling sets the gas temperature to $\sim 10^{3.8}$ K in the H II region (Osterbrock 1989). The structure of H II region has been studied in terms of the Balmer recombination lines of hydrogen atoms, the observations of other optical forbidden lines (e.g., [S II] $\lambda 6716$, [O II] $\lambda 3727$) (e.g., Peimbert et al. 1993; Peimbert 2003; Wang et al. 2004) and infra-red fine-structure lines (e.g., [O III] $88 \mu\text{m}$, [S III] $33 \mu\text{m}$) (e.g., Martín-Hernández et al. 2002). The theoretical advances have also been made by means of various photoionization models (e.g., Stasińska 1982; Ercolano et al. 2003; Morisset et al. 2005). Our understanding of the H II region has been advanced considerably in recent times with the aid of the Wisconsin H α Mapper (WHAM) data (Haffner et al. 2003). With a velocity resolution capability of 8–12 km/s, WHAM measured the H α emission from warm ionized objects within $\sim \pm 100 \text{ km s}^{-1}$ of the Local Standard of Rest and provided the first large-scale H α survey, covering the three-quarters of the northern sky. The survey results show that enhancements can generally be seen near the planetary nebulae and H II regions surrounding massive O and early B-type stars; the results also confirm the presence of unidentified high galactic components (Reynolds et al. 2005).

The α Vir (Spica), one of the brightest stars at a high galactic latitude, was found to be a double-lined spec-

troscopic binary with spectral types B1 V and B4 V (Herbison-Evans et al. 1971). The existence of the H II region around α Vir was suggested because the region appeared to be a hole in radio observations (Fejes 1974) and ultraviolet absorption lines were seen for the star of the nearby sightline (York & Kinahan 1979). Equipped with a Fabry-Perot spectrometer, Reynolds (1985) made H α scans and revealed that the region was indeed ionized with a gas density of $\sim 0.6 \text{ cm}^{-3}$. The hydrogen ionization rate of the whole H II region was estimated to be $\sim 10^{46.3}$ photons s^{-1} . The ratio of [S II] $\lambda 6716$ to the H α line, which signifies the contribution of collisional excitation with enhanced temperature, was also made for the Spica H II region (Spica Nebula). While the Spica Nebula is generally accepted as a normal H II region, the ratio was found to be rather high (0.16 at the center and 0.21 at the edge), compared to those of other H II regions such as the Orion Nebula (0.019, Peimbert & Torres-Peimbert 1977) and the Sharpless 261 (0.059, Hawley 1978), though its origin was not clearly identified (Reynolds 1988). Recently, the Spica Nebula was observed in the WHAM survey (Reynolds 2004), but no detailed study of this set of data has yet been published.

Si IV and C IV ion lines were detected in the far ultraviolet (FUV) absorption line study towards Spica, and their origin was ascribed to the Local Bubble (LB) surrounding the Sun (Savage & Wakker 2009). Being a photoionized H II region, the Spica Nebula may not be associated with these high-stage FUV lines, but it can still be a source of FUV emission from low-stage ions, especially in view of the high [S II] $\lambda 6716$ to H α line ratio. In this paper, we analyze the FUV Si II* and Al II emission lines as well as the WHAM survey data, to study the H II region around Spica. It should be noted that the ionization potentials of Si²⁺ and Al²⁺ are similar to that of hydrogen: 16.4 eV for Si²⁺ and 18.8 eV for Al²⁺. As the spatial structure of the Spica H II region was not explored previously and there have been no re-

¹ Korea Advanced Institute of Science and Technology (KAIST), 305-701 Daejeon, Republic of Korea; jwp@kari.re.kr

² Korea Aerospace Research Institute (KARI), 305-333 Daejeon, Republic of Korea

³ Korea Astronomy and Space Science Institute (KASI), 305-348 Daejeon, Republic of Korea

⁴ Space Sciences Laboratory, University of California, Berkeley, CA 94720, USA

ports of the emission line study in the FUV wavelengths, we believe the present study should provide useful information about the global morphology of the nebula. For the FUV study, we use the same data set as the one used for our previous analysis of Loop I superbubble (L1, Park et al. 2007); that data set was obtained from the Far-ultraviolet Imaging Spectrograph (FIMS) on the Korean microsatellite *STSAT-1* (Edelstein et al. 2006a). The FIMS is an instrument optimized for the measurement of diffuse FUV emissions with a large field of view (7.5×4.3) for the wavelength band of 1330–1720 Å. We also compare the observational results with the results of the Cloudy photoionization model so that we can constrain the physical parameters associated with the H II region and α Vir itself.

2. OBSERVATIONS

In Figure 1, we plot spectra for the three distinct regions of the Spica Nebula: the core region within 0.5° circle including the central point source, α Vir, in the top panel; the nebula region defined by $0.5^\circ - 8.0^\circ$ circle (Reynolds 1985) in the middle panel; and the background of a $12^\circ \times 12^\circ$ square outside the nebula in the bottom panel. The spectra were binned with 1 \AA and smoothed with a 3 \AA wide boxcar. For comparison, we also include in the top panel the spectrum for α Vir as observed by International Ultraviolet Explorer (*IUE*).

As can be seen in the top panel, the prominent absorption lines of Si IV $\lambda\lambda$ 1393.8, 1402.8 in the *IUE* spectrum, which undoubtedly originate from the stellar atmosphere, appear as strong emission lines in the diffuse FIMS spectrum; these lines indicate the extended hot gas around the central star. Similar features can also be identified for Si II* λ 1533.4 and the C IV doublet $\lambda\lambda$ 1548.2, 1550.8. However, as shown in the middle panel, the Si IV emission lines are not seen in the nebula region while Si II*, C IV doublet and Al II λ 1670.8 are bright. The C IV doublet is also conspicuous in the background region (bottom panel) while both the Si II* and Al II lines become less prominent compared to the nebula region. Hence, only the Si II* and Al II may actually be the dominant emission lines in the nebula region as the C IV doublet seen in the middle panel could be contributed from the projected background.

We have constructed FUV spectral images of the Spica Nebula (radius of $\sim 8^\circ$, Reynolds 1985), extended to $12^\circ \times 12^\circ$ to include the nearby background medium. The Si II* and Al II images were made by utilizing the HEALPix scheme (Górski et al. 2005) with a pixel resolution of ~ 0.92 . The Si II* and Al II lines were fitted with single Gaussian profiles in the spectral range 1520–1546 Å and 1658–1684 Å, respectively, for each pixel. The images were smoothed with a Gaussian function whose full width at half-maximum (FWHM) was 3° . The resulting signal to noise (S/N) ratios for the bright features of the nebula are above 3.0 for both Si II* and Al II.

Figure 2 shows the final Si II* and Al II images taken from FIMS. It also displays the $H\alpha$ image taken from Finkbeiner (2003) and the H I map taken from Kalberla et al. (2005). We designated α Vir in these images with an asterisk at $(RA, DEC) = (201.3, -11.2)$. The black circles with a radius of 8° , correspond to 12 pc

for a distance of 80 pc to α Vir; they indicate the region conventionally defined as the Spica Nebula (Reynolds 1985). First, we note that the Si II* image in Figure 2a shows an asymmetric feature with strong enhancement in the southern region below α Vir. The southern enhancement is also seen in the $H\alpha$ map of Figure 2c and seems to be related to the high neutral hydrogen density shown in Figure 2d. This asymmetric feature is less clear in the Al II map of Figure 2b; it does not show much difference between the northern and southern parts though the image seems to extend from the round-shaped central peak to the northwest direction, where the emission of $H\alpha$ is somewhat enhanced. In Figure 2c, we overplotted the H I contours from $2.0 \times 10^{20} \text{ cm}^{-2}$ to $8.0 \times 10^{20} \text{ cm}^{-2}$ with $2.0 \times 10^{20} \text{ cm}^{-2}$ intervals: $< 2.0 \times 10^{20} \text{ cm}^{-2}$ generally corresponds to the northern region above α Vir; $2.0 \times 10^{20} \sim 6.0 \times 10^{20} \text{ cm}^{-2}$ represents a band that passes through the southern H II region; and $> 6.0 \times 10^{20} \text{ cm}^{-2}$ represents the area below the Spica Nebula. In Figure 2d, a H I cavity is seen in the vicinity of α Vir which is probably generated by the strong Lyman continuum from the star that causes almost all of the neutral hydrogen atoms to be ionized.

We constructed radial profiles of the $H\alpha$, Si II* and Al II intensities for the Spica Nebula. Because the $H\alpha$ and Si II* images show strong asymmetry, we made the northern and southern intensity profiles separately by averaging the intensity for the corresponding concentric semicircles of 1° bins up to 8° . We subtracted the background radiation in these profiles: 1.4 Rayleigh (R) for $H\alpha$, the average value of the galactic latitudes between 40° and 60° (Reynolds 1984); 0.03 R for Si II* and 0.04 R for Al II where $1\text{R} = 8.0 \times 10^4 \text{ photons cm}^{-2} \text{ s}^{-1} \text{ sr}^{-1}$. We also made extinction corrections by using the extinction curve given by Cardelli et al. (1989) though the corrections are not significant. With an assumed $E(B-V)$ value of 0.01 for the H II region, the extinction corrected intensities of $H\alpha$, Si II* and Al II are respectively, about 1.02, 1.08 and 1.07 times the observed intensities (Galazutdinov et al. 2008).

The top panel in Figure 3 shows the resulting profiles. The solid line represents the northern profiles and dashed lines represents the southern profiles. The rather large error bars come from the significant spatial variation that still exists within each semicircle bin. As expected, in the $H\alpha$ and Si II* intensities we see a marked difference between the northern and southern regions with a much slower decrease for the southern profiles; in contrast, the Al II intensity does not show a marked difference between the northern and southern profiles. The southern $H\alpha$ profile even shows a flat region from 3 pc to 8 pc, which is undoubtedly due to the fact that the density increases with distance. The bottom panel in Figure 3 shows the model profiles obtained from a photoionization simulation and will be discussed in later section.

In Figure 4 we show a scatter plot of $N(\text{H I})$ against the $H\alpha$ intensity. A correlation is seen for $N(\text{H I})$ below $6.0 \times 10^{20} \text{ cm}^{-2}$ and the 0.62 correlation coefficient confirms that the $H\alpha$ enhancement in the southern Spica region can be attributed to that region's high neutral hydrogen density. Hence, the Spica Nebula is ionization-bounded in the southern region with an ionization front at $N(\text{H I}) = 6.0 \times 10^{20} \text{ cm}^{-2}$. The $H\alpha$ intensity drops significantly

to 1.6 R (Log $H\alpha=0.2$) for $N(\text{H I}) > 6.0 \times 10^{20} \text{ cm}^{-2}$ (Log $N(\text{H I})=20.78$); and the intensity drop implies that any H ionization photons that pass through this dense ambient medium are dissipated in the medium. It should be noted that the 1.6 R value that we obtained here is very similar to the average value (1.4 R) for the galactic latitudes between 40° and 60° , which were estimated by Reynolds (1984).

3. DISCUSSION

The observed intensity profiles of the northern and southern H II regions shown in the top panel of Figure 3 are compared with model calculations for the corresponding regions. When we ran the photoionization simulation code Cloudy, we varied the Lyman continuum luminosity, $Q(H)$, the effective temperature of the central star, and the density of the ambient medium. The simulation was performed for a spherically symmetric nebula by using the stellar atmospheric model of Castelli & Kurucz (2004) and by assuming the B star abundance reported by Kilian-Montenbruck et al. (1994) and Sembach et al. (2000). We obtained the volume emissivity as a function of the radius and calculated the intensity toward a line of sight defined by the offset angle from the central star. Finally, we smoothed the profiles with a Gaussian function whose FWHM was 3° for a direct comparison with the observations.

First, the calculation was performed for a constant density medium, corresponding to the northern region where density is more or less uniform. The results are shown as solid lines in the bottom panel of Figure 3. The model that fits best the northern $H\alpha$ profile was obtained with $Q(H) = 10^{46.2}$ photons s^{-1} , effective temperature of 26,000 K, and the density of 0.22 cm^{-3} . These values of $Q(H)$ and the effective temperature are quite similar to previous estimates of $10^{46.3}$ photons s^{-1} in Reynolds (1985) and 25,791 K in Kunzli et al. (1997), respectively. However, the density is much smaller than the result of 0.6 cm^{-3} estimated by Reynolds (1985), probably because the observation was made for the brightest portion of the nebula which is located in the central region. On the other hand, the model profiles of Si II* and Al II are quite different from the corresponding observed profiles, especially in the outer region beyond 3 pc, where the observed profiles show a much slower decrease with distance and have extended tails. In addition, the Al II model profile shows a much higher central peak intensity with a sharper decrease than the observed profile even inside 3 pc. These aspects will be discussed later, together with the results of the southern profiles.

Next, we modeled the southern region in which $N(\text{H I})$ is seen to increase outwards. As our goal was to study the general trends affected by the density gradient, not to reproduce the observed profiles exactly, we used the power-law model built in the code Cloudy, even though it may not represent the density profile accurately:

$$n(r) = n_c \left(\frac{r}{r_0}\right)^{-\alpha}, \quad (1)$$

where n_c is the density at r_0 , which was taken to be 0.3 pc. Best fit was obtained by matching the $H\alpha$ profiles with fixed $Q(H)$ and effective temperature from the simulation for the northern region. The resulting value is $\alpha = -0.15$ (corresponding to the density of 0.38 cm^{-3} at

$r = 12$ pc), and the model profiles are shown as dashed lines in the bottom panel of Figure 3. The $H\alpha$ fit looks more or less reasonable although the model shows a little higher central peak with a sharper decrease, which probably originates from the limits imposed by the power law profile of the model. However, the most significant discrepancies seem to be in the Si II* and Al II profiles. For example, the model Si II* profile does not show such an enhancement as the one seen in the observed profile region between 2 pc and 8 pc, not responding to the outward density increase. The density gradient effect is not manifested in the model Al II result, either, with a profile very similar to that of the northern region. In fact, for Al II, both the northern and southern observations look similar, with smaller central peaks and broader profiles than the models.

Hence, several discrepancies exist between the observation results and those of a simple photoionization model such as Cloudy. For example, the observed Si II* and Al II profiles show extended tails not reproduced by Cloudy. The observed Si II* profile shows the effect of the increasing density gradient in the southern region of the nebula while the model does not reproduce the feature. The observed Al II profile, compared to the model profile, is significantly broader with a much smaller central peak (about 25% of the model). In addition, the observed Al II profile does not respond to the density gradient. We would like to discuss these peculiar features here. First, we believe the extended tails seen in the observed profiles are caused by the background of enhanced temperature. Figure 1 clearly shows the existence of the C IV doublet in the nebula regions as well as in the background, which can hardly be produced by photoionization in H II regions. It should also be noted that Si IV and C IV ions were detected recently towards Spica (Savage & Wakker 2009). We will argue later that the Spica Nebula is located close to the interface between the L1 and LB, which contain hot gases. In addition to this background hot gas, the Spica Nebula may actually be embedded in a medium of enhanced temperature. The temperature profile obtained from our photoionization model for the southern region of the nebula shows a temperature drop from $\sim 5,000$ K to $\sim 3,000$ K with a change in distance from 1 pc to 4 pc, while it remains more or less at $\sim 5,000$ K in the northern region. In this regard, it should be noted that the ratio of [S II] $\lambda 6716$ to the $H\alpha$ line was observed to be rather high in the Spica Nebula region with its value of 0.21 at $(RA, DEC) = (205^\circ 3, -11^\circ 1)$ (Reynolds 1988), as mentioned previously. Assuming the general line ratio of 1.3 for [S II] $\lambda 6716/\lambda 6731$ (Chanot & Sivan 1983), the [S II] $\lambda\lambda 6716 + 6731/H\alpha$ is estimated to be 0.36. This value is rather high for a photoionized H II region and actually resides between those of a general H II region and a mixing layer of shocked gases (Lasker 1977). We suspect that the model Si II* profile would have been more responsive to the density increase if the ambient medium were assumed to be of enhanced temperature, the situation which the present Cloudy model does not simulate.

The enhanced temperature may also cause broadening of the observed Al II profile. However, the profile, both in the observation and in the model, does not show north-south asymmetry. Moreover, the observed

central peak is much smaller than that expected from the model. We believe this discrepancy originates from the multiple resonant scattering of Al II in the nebula, which is not properly considered in the photoionization model Cloudy. The resonance lines, such as Al II, undergo many resonant scattering events, resulting in a much longer random walk before they can escape the nebula. The numerous scatterings can yield a consequently higher probability of being absorbed by dust. While detailed calculation requires extensive scattering simulations which are not pursued here, a simple estimation would demonstrate reduction of Al II intensity to the observed value. Using the Al⁺ column density 13.05 cm⁻² and the average nebular temperature 10^{3.6} K obtained from the current photoionization model, the optical depth of the resonance scattering of Al II is estimated to be 22.9 (Verhamme et al. 2006). The number of scattering within a medium would be approximately given by $N_{\text{scatt}} \approx \max(\tau, \tau^2)$ (Rybicki & Lightman 1979). Then, the total path length of the random walking photons would be $L_{\text{tot}} \approx N_{\text{scatt}} \times L/\tau = L \times \max(1, \tau)$, where L is the typical nebular size, and the resonant lines would experience τ times higher dust-extinction than that of the original nebular size ($\tau > 1$). Adopting $E(B-V) = 0.01$ (Galazutdinov et al. 2008), the dust-extinction optical depth of Al II is 1.47, and thereby only $\sim 23\%$ of Al II line would escape from the nebula, and the value is roughly consistent with the observed peak intensity. Another effect of this multiple scattering is of course broadening of the radial profile as the photons diffuse out radially through random walks. The effect of increasing density in the southern region may also have become obscured due to this diffusion.

We further note that the ground state of the singly ionized ion Si⁺ is split. The emission lines from the excited state $3s^2 4s^1 \ ^2S_{1/2}$ to the true ground state $3s^2 3p^1 \ ^2P_{1/2}$ (Si II, 1527Å) and to the excited ground state $3s^2 3p^1 \ ^2P_{3/2}$ (Si II*, 1533Å) has a transition ratio of 1 : 2. The true Si II $\lambda 1527$ ground state transition is optically thick and therefore undetectable (Korpela et al. 2006). Adopting the same way for the Al II, the optical depth of the resonance line Si II is estimated to be 12.6. How-

ever, resonantly absorbed Si II make downward transitions with the line ratio of 1 : 2 between Si II and Si II*, most of Si II are converted to Si II* after only a few resonance scatterings, which halts further resonant scattering ($N_{\text{scatt}} = 2; I_{1527}/I_{1533} \approx 0.04$). Therefore Si II* would not be significantly reduced by dust absorption.

As mentioned above, the southern enhancement in the Spica Nebula is clearly associated with the dense H I region shown in Figure 2d, in which $N(\text{H I})$ increases from less than 2×10^{20} to over 7×10^{20} cm⁻². This H I shell bounding the ionization front was initially suggested to be a H I cloud by Fejes (1974). However, we would like to note that this H I shell coincides with the region of interaction between the L1 and LB, called “interaction ring” (IR) (Egger & Aschenbach 1995). The estimated distance to the IR (~ 70 pc) is comparable to that of the Spica Nebula (68–92 pc, Reynolds 1985). Extended morphology of the IR near the Spica was recently discussed in Park et al. (2007). The result indicates that the warm ionized gas in the Spica Nebula was possibly created in the already disturbed medium by the IR which affects the evolution of the H α region significantly.

4. CONCLUSION

The H α distribution as well as those of Si II* and Al II obtained in the FUV wavelengths was analyzed for a $12^\circ \times 12^\circ$ sky around the Spica Nebula. The spatial variation, shown in both H α and Si II* images, confirmed that the Spica Nebula is bounded by a high density H I shell in the southern region which we relate to the “interaction ring” of the L1 and the LB. We have also argued that the nebula is possibly embedded in a gas of enhanced temperature, based on that the observed emission profiles have long extended tails and they respond to the density increase in the southern region of the nebula, which is not explained by photoionization only.

The *IUE* data presented in this paper were obtained from the Multimission Archive at the Space Telescope Science Institute (MAST). STScI is operated by the Association of Universities for Research in Astronomy, Inc., under NASA contract NAS5-26555. Support for MAST for non-HST data is provided by the NASA Office of Space Science via grant NAG5-7584 and by other grants and contracts.

REFERENCES

- Cardelli, J. A., Clayton, G. C., & Mathis, J. S. 1989, *ApJ*, 345, 245
- Castelli, F., & Kurucz, R. L. 2004, arXiv:astro-ph/0405087
- Chanot, A., & Sivan, J. P. 1983, *A&A*, 121, 19
- Edelstein, J., et al. 2006a, *ApJ*, 644, L153
- Egger, R. J., & Aschenbach, B. 1995, *A&A*, 294, L25
- Ercolano, B., Barlow, M. J., Storey, P. J., & Liu, X.-W. 2003, *MNRAS*, 340, 1136
- Fejes, I. 1974, *AJ*, 79, 25
- Ferland, G. J., Korista, K. T., Verner, D. A., Ferguson, J. W., Kingdon, J. B., & Verner, E. M. 1998, *PASP*, 110, 761
- Finkbeiner, D. P. 2003, *ApJS*, 146, 407
- Galazutdinov, G. A., Lo Curto, G., & Krelowski, J. 2008, *MNRAS*, 386, 2003
- Górski, K. M., Hivon, E., Banday, A. J., Wandelt, B. D., Hansen, F. K., Reinecke, M., & Bartelmann, M. 2005, *ApJ*, 622, 759
- Haffner, L. M., Reynolds, R. J., Tufte, S. L., Madsen, G. J., Jaehnig, K. P., & Percival, J. W. 2003, *ApJS*, 149, 405
- Hawley, S. A. 1978, *ApJ*, 224, 417
- Herbison-Evans, D., Hanbury Brown, R., Davis, J., & Allen, L. R. 1971, *MNRAS*, 151, 161
- Kalberla, P. M. W., Burton, W. B., Hartmann, D., Arnal, E. M., Bajaja, E., Morras, R., Pöppel, W. G. L. 2005, *A&A*, 440, 775
- Kilian-Montenbruck, J., Gehren, T., & Nissen, P. E. 1994, *A&A*, 291, 757
- Korpela, E. J., et al. 2006, *ApJ*, 644, L163
- Kunzli, M., North, P., Kurucz, R. L., & Nicolet, B. 1997, *A&AS*, 122, 51
- Lasker, B. M. 1977, *ApJ*, 212, 390
- Martín-Hernández, N. L., et al. 2002, *A&A*, 381, 606
- Morisset, C., Stasińska, G., & Peña, M. 2005, *MNRAS*, 360, 499
- Osterbrock, D. E. 1989, Research supported by the University of California, John Simon Guggenheim Memorial Foundation, University of Minnesota, et al. Mill Valley, CA, University Science Books, 1989, 422 p.
- Park, J.-W., et al. 2007, *ApJ*, 665, L39
- Peimbert, M., & Torres-Peimbert, S. 1977, *MNRAS*, 179, 217
- Peimbert, M., Storey, P. J., & Torres-Peimbert, S. 1993, *ApJ*, 414, 626

- Peimbert, A. 2003, ApJ, 584, 735
Reynolds, R. J. 1984, ApJ, 282, 191
Reynolds, R. J. 1985, AJ, 90, 92
Reynolds, R. J. 1988, ApJ, 333, 341
Reynolds, R. J. 2004, AdSpR, 34, 27 Tufte, S. L., Haffner, L. M., Jaehnig, K., & Percival, J. W. 1998, Publications of the Astronomical Society of Australia, 15, 14
Reynolds, R. J., Chaudhary, V., Madsen, G. J., & Haffner, L. M. 2005, AJ, 129, 927
Rybicki, G. B., & Lightman, A. P. 1979, New York, Wiley-Interscience, 1979. 393 p.
Savage, B. D., & Wakker, B. P. 2009, ApJ, 702, 1472
Sembach, K. R., Howk, J. C., Ryans, R. S. I., & Keenan, F. P. 2000, ApJ, 528, 310
Stasińska, G. 1982, A&AS, 48, 299
Verhamme, A., Schaerer, D., & Maselli, A. 2006, A&A, 460, 397
Wang, W., Liu, X.-W., Zhang, Y., & Barlow, M. J. 2004, A&A, 427, 873
York, D. G., & Kinahan, B. F. 1979, ApJ, 228, 127

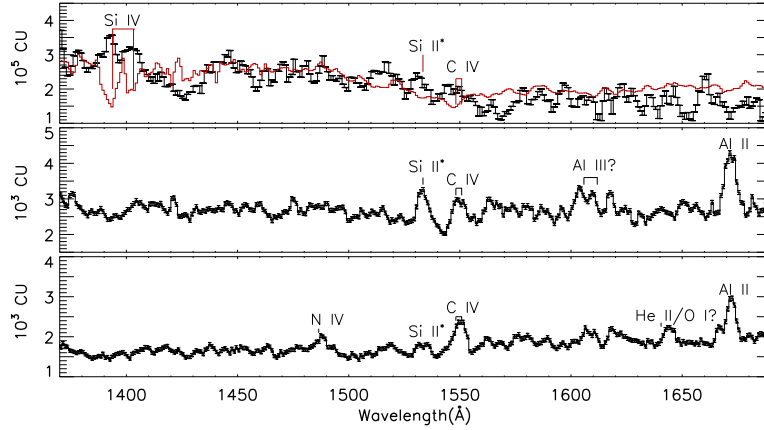


FIG. 1.— FUV Spectra of the Spica Nebula: the core region within $0^{\circ}5$ (top panel), the nebula region of $0^{\circ}5 - 8^{\circ}0$ (middle panel), and the background of $12^{\circ} \times 12^{\circ}$ square outside the nebula (bottom panel). The spectrum of the central star observed by *IUE* is also plotted in red in the top panel. Several ion lines are marked in the figure. The spectra were binned with 1 \AA and smoothed with a boxcar whose width is 3 \AA . NOTE.- $\text{CU} = \text{photons s}^{-1} \text{ cm}^{-2} \text{ sr}^{-1} \text{ \AA}^{-1}$

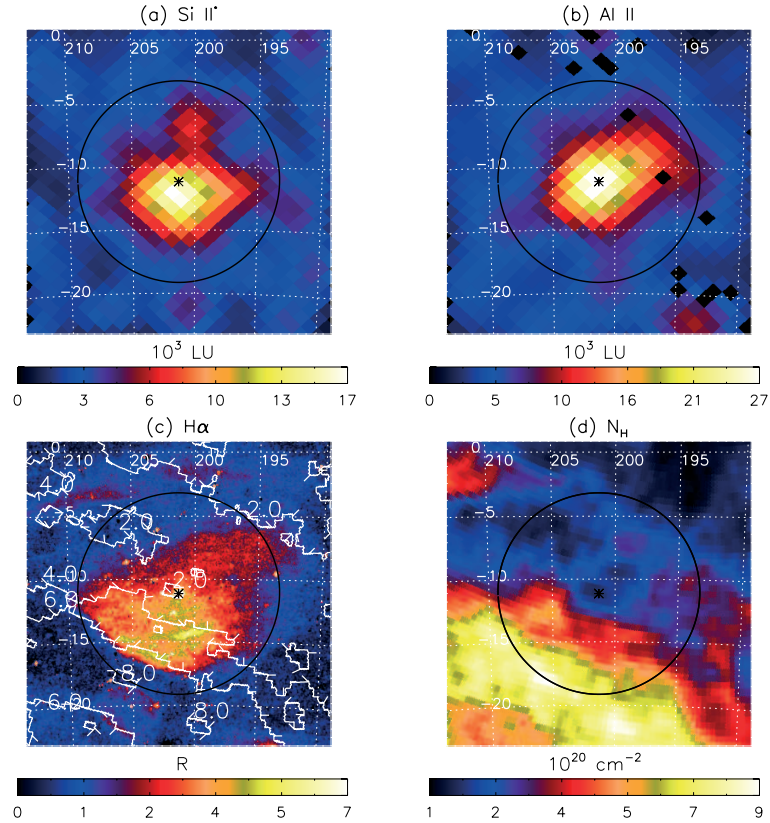


FIG. 2.— Spectral images of the Spica H II region: (a) FIMS Si II*; (b) FIMS Al II; (c) WHAM $\text{H}\alpha$ (Finkbeiner 2003); and (d) N_H map (Kalberla et al. 2005). The large black circles of radius of 8° in (a) - (d) indicate the region conventionally defined as the Spica Nebula. The N_H contours are overlaid in (c). NOTE.- $\text{LU} = \text{photons s}^{-1} \text{ cm}^{-2} \text{ sr}^{-1}$

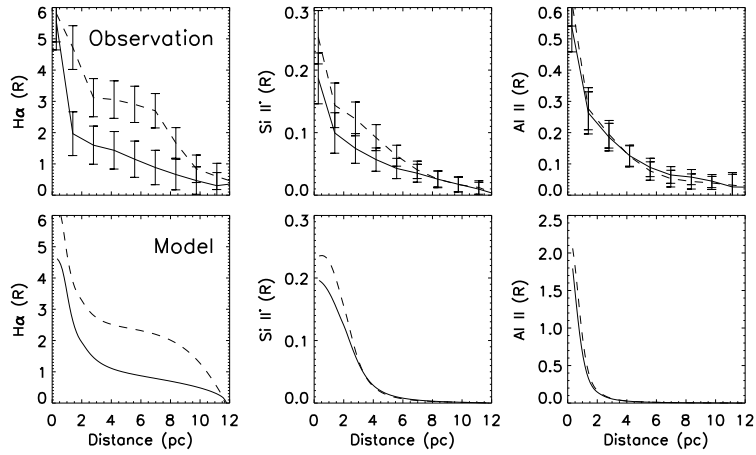


FIG. 3.— Radial profiles of the $H\alpha$, Al II and Si II* for the Spica Nebula. Top panel shows the observed profiles with 1 sigma error bars for the northern (solid lines) and southern (dashed lines) regions. The results of the spectral synthesis models for the corresponding northern and southern regions are shown in the bottom panel.

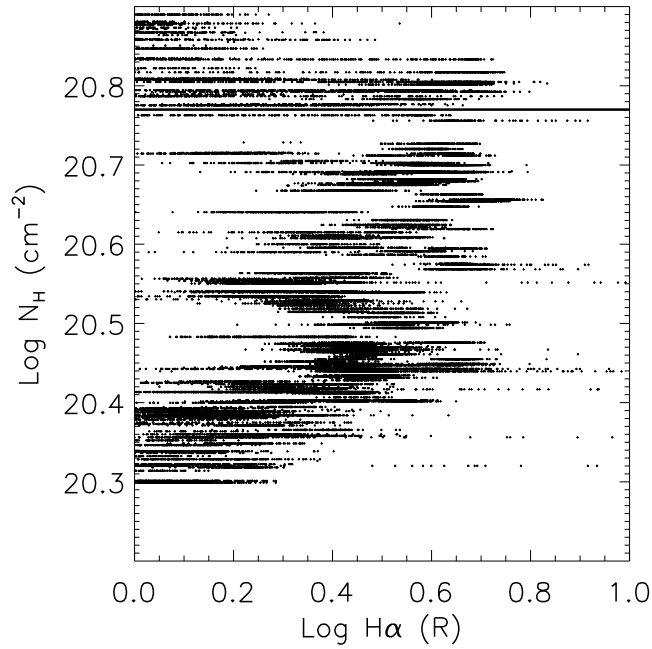


FIG. 4.— $N(\text{H I})$ is plotted against $H\alpha$ in the logarithmic scale for the Spica Nebula region 8° . Correlation is seen for $N(\text{H I})$ below $6.0 \times 10^{20} \text{ cm}^{-2}$ (marked as a black horizontal line). These data points represent the correlation coefficient of 0.62.